ARTICLES

Journal of Semiconductors
(2020) 41, 072901
doi: 10.1088/1674-4926/41/7/072901

Growth of large-scale two-dimensional insulator $Na_2Ta_4O_{11}$ through chemical vapor deposition

Yuanyuan Jin, Huimin Li†, and Song Liu†

Institute of Chemical Biology and Nanomedicine (ICBN), State Key Laboratory of Chem/Bio-Sensing and Chemometrics, College of Chemistry and Chemical Engineering, Hunan University, Changsha 410082, China

Abstract: The insulator $Na_2Ta_4O_{11}$ has been considered as a potential photocatalyst. However, little attention has been given to the synthesis of $Na_2Ta_4O_{11}$ nanoparticles, let alone the growth of two-dimensional (2D) layered $Na_2Ta_4O_{11}$ flake, which may bring innovative properties and promising applications. Here, the 2D thin-layer $Na_2Ta_4O_{11}$ flake was first produced by chemical vapor deposition (CVD) method, with the smallest thickness reported currently. We have also synthesized 2D $Na_2Ta_4O_{11}$ flake over 100 μm, which was the largest value over the 2D level reported to date. Our work proposed novel strategies to synthesize other 2D metal oxide material and endow the $Na_2Ta_4O_{11}$ more properties and applications.

Key words: $Na_2Ta_4O_{11}$; two-dimensional materials; chemical vapor deposition; insulator

Citation: Y Y Jin, H M Li, and S Liu, Growth of large-scale two-dimensional insulator $Na_2Ta_4O_{11}$ through chemical vapor deposition[J]. *J. Semicond.*, 2020, 41(7), 072901. http://doi.org/10.1088/1674-4926/41/7/072901

1. Introduction

The photocatalytic metal-oxides have attracted considerable attention thanks to their outstanding properties and applications. The solar power can be utilized to drive fuel-generating reactions, such as the photocatalytic water-splitting[1, 2]. Among these metal-oxides, tantalate (Ta)-based photocatalysts such as $NaTaO_3$ has been of much interest because of its high quantum efficiency[3–5], which can be up to about 56%[6]. $Na_2Ta_4O_{11}$ is another type of sodium tantalite. The structure and tantalum coordination environment of $Na_2Ta_4O_{11}$ are different from $NaTaO_3$, which provide various insights into its optical and photocatalytic properties. $Na_2Ta_4O_{11}$ crystal has been shown to be an insulator with an indirect bandgap of 3.63 eV[7]. Its space group is R3c and is included in a rhombohedral system. The lattice parameters were a = 0.62086 nm and c = 3.6618 nm[8]. Ratnamala *et al.* reported that $Na_2Ta_4O_{11}$ acted as a photocatalyst to promote a water splitting reaction[9]. To advance the exploration towards its fundamental physical properties, the synthesis of $Na_2Ta_4O_{11}$ will be essential. Flux synthetic and sol-gel are the main approaches. For example, McLamb *et al.* prepared large single-crystal $Na_2Ta_4O_{11}$ particles with a K_2SO_4/Na_2SO_4 flux at a temperature of 1000 °C for 2 h[10]. In Katsuya Teshima's study, $Na_2Ta_4O_{11}$ crystal was grown in $Na_2Mo_2O_7$ flux via a slow-cooling method [11].

However, these methods have always produced impure crystal because they were grown in air, and the direct preparation of product *in situ* led to mixed reactants and products. Furthermore, these methods obtained either bulk $Na_2Ta_4O_{11}$ crystals or small crystals. To date, there has been no study on the growth of thin-layered $Na_2Ta_4O_{11}$, which will be essential to explore its optical properties. Chemical vapor deposition (CVD) is a powerful technology to synthesize large-scale two-dimensional (2D) materials. CVD is a process in which the chemical reactions between gaseous substances occurred, and subsequently produced solid sediments on the substrate[12–14]. The CVD method can not only control the thickness and size of materials but also prepare crystals with higher purity[15–17]. Based on this, we believe that the CVD method is suitable for the preparation of large and thin $Na_2Ta_4O_{11}$, which endows it with high crystallinity for more potential applications.

Here, by using Na_2SO_4 and Ta_2O_5 as precursor, we first applied the CVD method to prepare large and thin-layered $Na_2Ta_4O_{11}$ flake. The structure of $Na_2Ta_4O_{11}$ flakes were characterized by X-ray diffraction (XRD), energy dispersive X-ray spectroscopy (EDS), and Raman techniques, indicating the successful synthesis of $Na_2Ta_4O_{11}$. The atomic force microscope (AFM) demonstrated the thickness reached ~5.2 nm, which was the thinnest $Na_2Ta_4O_{11}$ reported so far. High resolution transmission electron microscopy (HRTEM) revealed its high crystallinity and quality. Moreover, we observed that the growth time had strong effects on crystal size and thickness. Our work first synthesized thin-layer $Na_2Ta_4O_{11}$, which paved the way for further exploration of its potential properties and applications.

2. Experiments

2.1. Growth of $Na_2Ta_4O_{11}$

The growth was performed with a single temperature heating system, which was a 30 cm one-zone furnace system. Na_2SO_4 powder (14.2 mg, 99.5%, Sinopharm Chemical Reagent Co., Ltd) mixed with Ta_2O_5 powder (39.4 mg, 99.9%, Sigma Aldrich) were put into a crucible, which was placed at the highest temperature zone. A sapphire substrate was placed facedown above the mixed powders. Then the center of the furnace was heated to 850 °C for 43 min (the rate was

Correspondence to: H M Li, huiminli@hnu.edu.cn; S Liu, liusong@hnu.edu.cn
Received 23 MARCH 2020; Revised 4 APRIL 2020.
©2020 Chinese Institute of Electronics

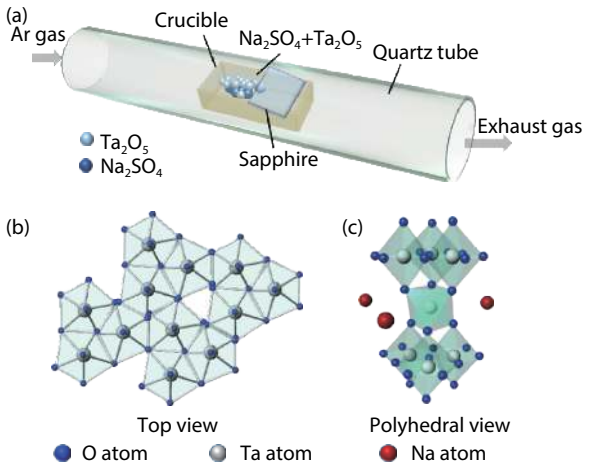

Fig. 1. (Color online) Synthesis of thin $Na_2Ta_4O_{11}$ flakes via CVD setup and crystal structure of $Na_2Ta_4O_{11}$. (a) Schematic diagram of the CVD setup used for synthesis of $Na_2Ta_4O_{11}$ flakes. (b) Top view of a single layer of TaO_7 pentagonal bipyramids. (c) Polyhedral view of the local coordination environments in $Na_2Ta_4O_{11}$ for a single TaO_6 octahedron. The O, Ta and Na atoms are represented by blue, silver and red balls, respectively.

20 °C/min), which held for 30 min at 850 °C under 100 sccm high-purity (99.9999%) argon atmosphere. After growth, the tube was cooled naturally.

2.2. Characterization

SEM (Hitachi-S4800) combined with EDS was applied to characterize morphology and elemental composition. AFM (Bruker Dimension Icon) was used to measure the thickness. Raman analysis was conducted under the excitation of a 532 nm laser, which executed with an inVia confocal Renishaw Raman spectrometer. HRTEM (Tecnai G2 F20 S-TWIN) analysis was performed to investigate the structure on an atomic scale. The acceleration voltage was 60 kV to avoid damage samples. Element identification was acquired by using XPS (AXIS-165) equipped with a monochromatic Al K_α source (λ = 1486.6 eV). XRD (Bruker Dimension Icon D8 Advance system) measurements were performed by using Cu K_α radiation (40 kV, 40 mA).

3. Results and discussion

Fig. 1(a) illustrates the CVD setup. In brief, a crucible filled with mixture of Na_2SO_4 and Ta_2O_5 was placed in the center of heating zone. The corresponding molar ratio of precursors was 1 : 1. A sapphire substrate was loaded face down on top of the powder. Then, the heating zone was heated to 850 °C for 43 min (the rate was ~20 °C/min), which held for 30 min at 850 °C under 100 sccm high-purity (99.9999%) argon atmosphere. After growth, the furnace was cooled to room temperature. The growth details are depicted in the experimental section. The $Na_2Ta_4O_{11}$ presented bilayer structure: a distort TaO_7 pentagonal bipyramid layer, which alternated with another layer of isolated TaO_6 octahedra[18]. Fig. 1(b) displayed the top view of a single layer of TaO_7 pentagonal bipyramids. Fig. 1(c) shows the polyhedral view of a single TaO_6 octahedron, which bond with six edge-sharing pentagonal bipyramids, and the Na^+ cations partially occupied an irregular seven-coordinate site. This structure functions as a repeated unit cell to bond with another same structure for regular arrange, forming the $Na_2Ta_4O_{11}$ crystal[19].

Considering prior works, we deduced the reaction process between Na_2SO_4 and Ta_2O_5, involving two steps[20]. First, Na_2SO_4 was thermally decomposed to Na_2O with the gaseous product of SO_2/SO_3, plus some other volatile compounds. Second, under appropriate thermodynamic conditions, the formed Na_2O in step one dissolved Ta_2O_5 to generate $Na_2Ta_4O_{11}$. The reactions are presented as following chemical equations:

$$Na_2SO_4\,(s) = Na_2O\,(s) + SO_2\,(g) + \frac{1}{2}O_2\,(g)\,, \qquad (1)$$

$$Na_2O\,(s) + 2Ta_2O_5\,(s) = Na_2Ta_4O_{11}\,(s)\,. \qquad (2)$$

Typically, the as-grown $Na_2Ta_4O_{11}$ flakes are triangles and hexagons. Fig. 2(a) displays the representative optical images of triangle $Na_2Ta_4O_{11}$, in which the length of thin-layer flake was measured to be ~5.5 μm. It was obvious that each triangle flake showed a different color, revealing the varied thickness, in which the brighter triangles indicates thicker flakes and the darker ones represents thinner flakes (marked with red and yellow, respectively). Then, AFM was conducted to analyze the coarseness and height of representative thin flake (Fig. 2(b)). The height diagram revealed a thickness of ~5.2 nm, which was one of the smallest reported values. The corresponding AFM image indicated a flat and uniform surface of thin-layer $Na_2Ta_4O_{11}$. Structure confirmation of $Na_2Ta_4O_{11}$ was determined by XRD characterization (Fig. 2(c)), in which the result showed that positions of all diffraction peaks were consistent with the standard peaks of $Na_2Ta_4O_{11}$. Strong and sharp peaks were observed, almost without the peaks of impurities, indicating the high crystallinity of $Na_2Ta_4O_{11}$. It is noted that there is a strong peak at ~ 41.7°, which is assigned to the peak of the substrate of sapphire. Fig. 2(d) shows the Raman spectroscopy of $Na_2Ta_4O_{11}$ excited with a 532 nm laser at room temperature. Six strong peaks are located at 224.5, 240.8, 294.8, 611, 661, and 1328.3 cm^{-1}, respectively. The peak at 410 cm^{-1} belongs to the A_{1g} mode of sapphire substrate. Although it was difficult to compare with other work due to the lack of previous studies about the Raman peak of $Na_2Ta_4O_{11}$, we can still almost determine that these six strong peaks belong to the $Na_2Ta_4O_{11}$ flake based on the confirmation of XRD.

Figs. 3(a)–3(c) show the X-ray photoelectron spectroscopy (XPS) spectra of Na 1s, O 1s, and Ta 4f, ascertaining the state of each element in $Na_2Ta_4O_{11}$. A strong single peak at 1071.9 eV is consistent with Na^+ (Fig. 3(a))[21]. The peak at binding energies (BEs) of 531.1 eV was assigned as O 1s (Fig. 3(b))[22]. The Ta-related peaks of Ta $4f_{7/2}$ and Ta $4f_{5/2}$ were located at BEs of 22.7, 23.9, 26.0, and 28.0 eV (Fig. 3(c)), respectively, which was in the range of reported Ta state[23]. It can be determined that there were two types of Ta state, based on the analysis and reported work, in which the blue peaks indicated Ta^{5+} state, and the yellow peaks represented the Ta^{2+} state. The Ta^{2+} was possibly due to the reduction of Ta^{5+} by sulfur gas, which released from the thermal decomposition of Na_2SO_4[20]. However, the exposure of crystal to the atmosphere prior to characterization created large amount of oxygen, plus the oxygen composition of sapphire substrate (Al_2O_3), resulting in the stoichiometric ratio of Na, Ta and O

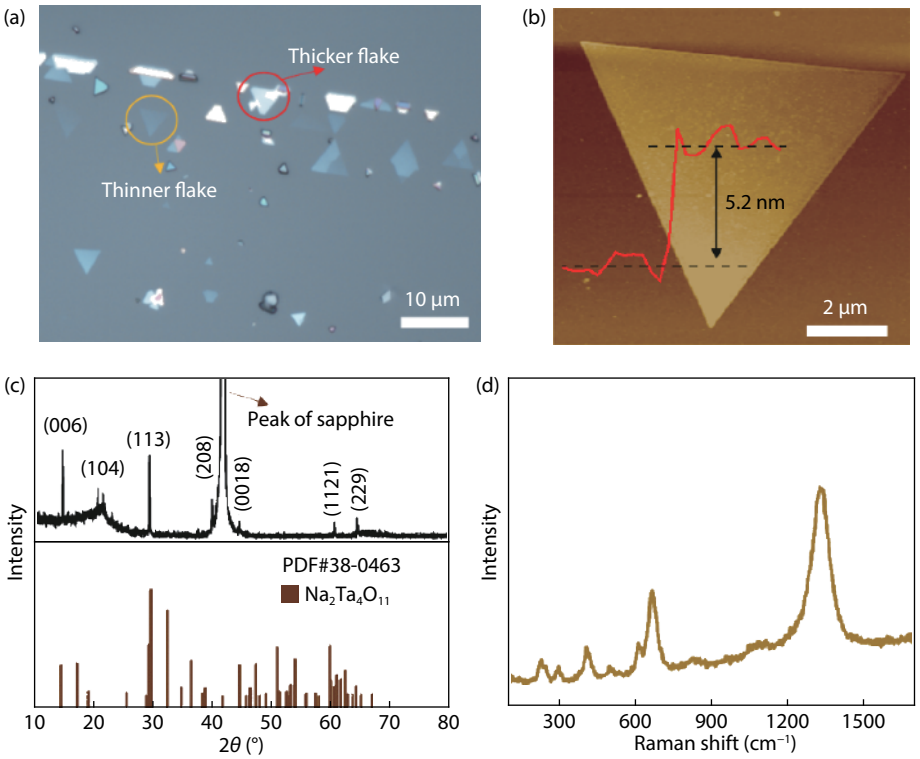

Fig. 2. (Color online) Characterizations of CVD-grown thin $Na_2Ta_4O_{11}$ flakes. (a) Representative optical image. (b) AFM characterization. (c) XRD characterization. (d) Typical Raman spectra of $Na_2Ta_4O_{11}$ flakes.

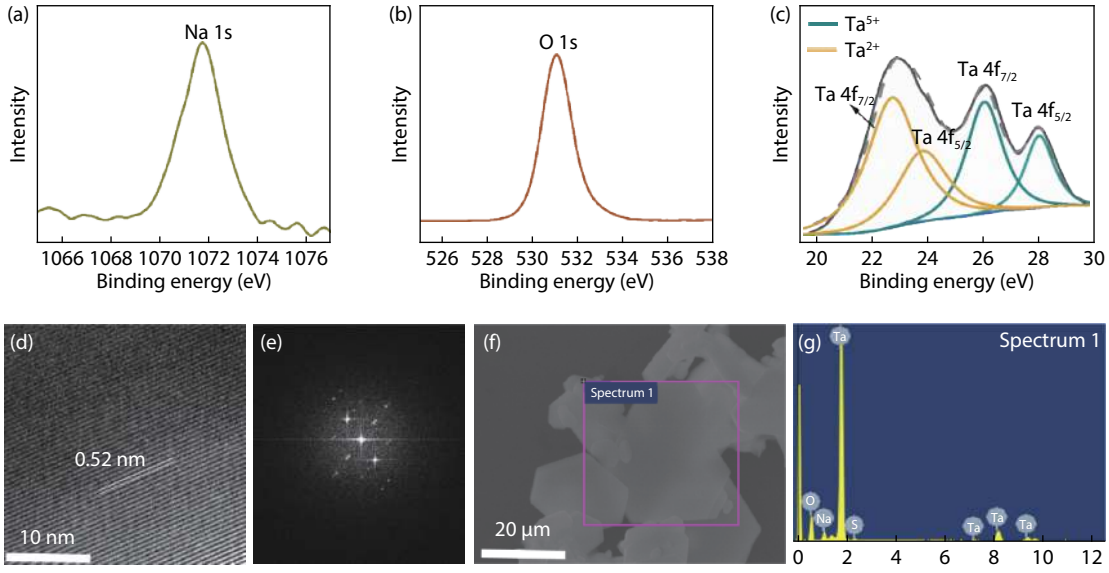

Fig. 3. (Color online) Structure characterization of CVD-grown $Na_2Ta_4O_{11}$ flakes on sapphire. XPS core level spectra of (a) Na 1s, (b) O 1s, and (c) Ta 4f. (d) HRTEM image and (e) FFT pattern image of thin $Na_2Ta_4O_{11}$ flakes. (f) SEM image for analysis of EDS. (g) The corresponding EDS spectra of the $Na_2Ta_4O_{11}$ flake in (f).

beyond 2 : 4 : 11. Hence, information about the atomic ratio cannot be further extracted from XPS.

We then performed HRTEM technology to characterize the crystalline structure of flake, and the flake was transferred on TEM grid using the poly(methyl methacrylate) (PMMA)-assisted method[24]. With an acceleration voltage of 60 kV, a HRTEM image with regular stripes was given (Fig. 3(d)). All of the stripes were aligned in the same direction and with the same lattice spacing, indicating the single crystal nature of $Na_2Ta_4O_{11}$ flake. The interplanar spacing was measured to be ~0.52 nm, consistent with the lattice constant of (012) plane. Fig. 3(e) presents the corresponding post-processed fast Fourier transformation (FFT) image-processed by the Gatan Digital Micrograph software. It is clear that adjacent bright spots form a hexagon, and the measured specific interplanar distances of 5.2 Å assigned to the (012) planes, which further confirms the high crystallinity of $Na_2Ta_4O_{11}$. In Fig. 3(g), the EDS image shows the peaks of Ta, Na and O with a little impurity of S, which confirms the chemical composition of $Na_2Ta_4O_{11}$. A small peak of S was possibly

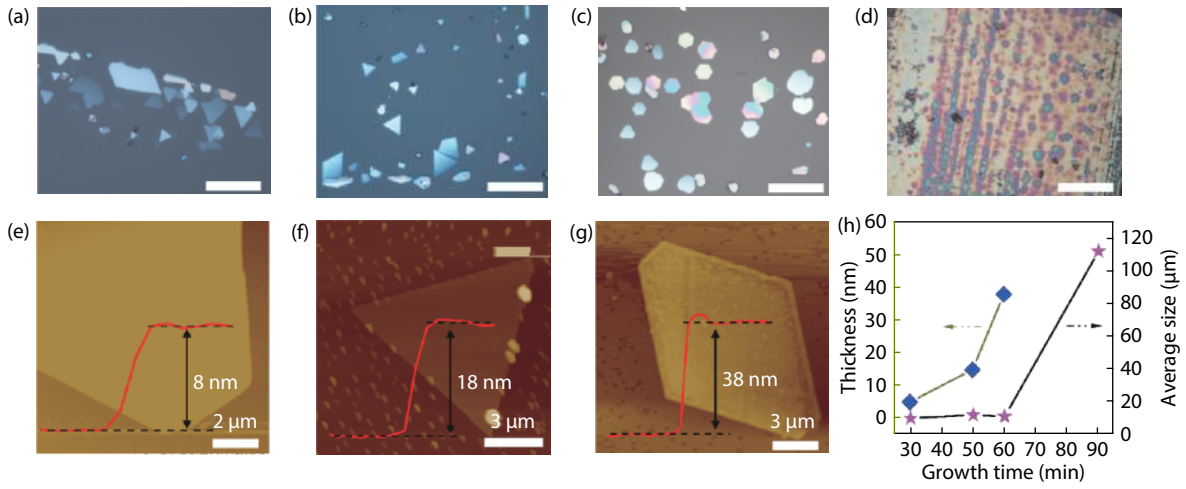

Fig. 4. (Color online) Deposition time-dependent optical images of $Na_2Ta_4O_{11}$ flake. (a–d) Optical images of $Na_2Ta_4O_{11}$ with deposition time at 30, 50, 60, and 90 min. Scale bars: 20 μm. (e–g) Representative AFM images of $Na_2Ta_4O_{11}$ flake with deposition time from 30 to 60 min. (h) Average size (purple star) and thickness (blue square) as a function of growth time.

caused by the deposition of a small amount of Na_2SO_4 on the flake surface. The performance of the $Na_2Ta_4O_{11}$ flake would not be affected because the impurities can be dissolved in water or aqua regia without destroying the structure of the flake. The zone selected by the purple box in Fig. 3(f) displays the hexagonal $Na_2Ta_4O_{11}$ flake. We used this region to collect element information in the EDS characterization.

These results demonstrate that the growth of thin-layer $Na_2Ta_4O_{11}$ with CVD method worked extremely well. Of the governing parameters in this work, growth time was an important parameter for $Na_2Ta_4O_{11}$ growth. At a growth temperature of 850 °C with molar ratio (Na_2SO_4 : Ta_2O_5) of 1 : 1, the growth time varied from 30 to 90 min. The optical images of flakes grown on sapphire corresponding to the deposition time of 30, 50, 60, and 90 min are presented in Figs. 4(a)–4(d). It is clear that the main morphology of $Na_2Ta_4O_{11}$ flake is hexagonal and triangular. No substantial change of crystal size was shown before the growth time of 60 min. For longer growth time of 90 min, the interconnected $Na_2Ta_4O_{11}$ flakes grow into a continuous film, which was measured to be 112 μm. At the boundary of the continuous film, we can observe several isolated triangles. This indicates that the formation of the film was initiated from the complete coalescence of flakes. Then AFM characterization was applied to measure the representative thickness of flakes grown at 30, 50, and 60 min, the results are shown in Figs. 4(e)–4(g). The AFM characterization of flakes at growth time of 90 min is not shown because of its height difference: it was thicker than the flakes obtained at a growth time of 60 min. These results can be evidenced by the color evolution of the $Na_2Ta_4O_{11}$ flake. It is clear that the longer deposition time led to a thicker flake. Thickness increased with time without substantial size change before 60 min, which may result from the stronger chemical reactivity and lower energy barrier of $Na_2Ta_4O_{11}$ surface when compared to the sapphire surface. Consequently, it resulted in a stack growth on thin $Na_2Ta_4O_{11}$ flake surface instead of epitaxial lateral growth. The average size and thickness of $Na_2Ta_4O_{11}$ as a function of growth time is illustrated in Fig. 4(h). In this case, the growth time of 60 min was a turning point to control the growth model of vertical stack growth and coalescence of flakes. We speculate that new seeding molecules were likely to deposit on the top of the bottom layer because of its low thermodynamic barrier on the surface. This barrier increased with thickness, thus $Na_2Ta_4O_{11}$ molecules would tend to nucleate on the substrate surface and form new stacked grown $Na_2Ta_4O_{11}$ flakes. Subsequently, adjacent $Na_2Ta_4O_{11}$ flakes integrated with each other to form a large film.

This study is the first work to grow large 2D $Na_2Ta_4O_{11}$, which is important for researching its potential application and properties. The physical properties of $Na_2Ta_4O_{11}$ change dramatically from three dimensional (3D) to 2D because electrons were confined to nanoscale motion in two dimensions[25], hence the synthesis of 2D $Na_2Ta_4O_{11}$ would expand its performance. Furthermore, 2D $Na_2Ta_4O_{11}$ is an insulator material with a very large specific surface area, which may be used as a high-performance load or filter material for promising applications in micro-nano photoelectric catalysis.

4. Conclusion

In conclusion, thin $Na_2Ta_4O_{11}$ flakes were first successfully prepared by the CVD method on sapphire substrate. The structure and growth of $Na_2Ta_4O_{11}$ flakes were confirmed with comprehensive characterization approaches. Controllable thickness and size by regulating growth time gave evidence that the CVD method has advantages in controlling growth of $Na_2Ta_4O_{11}$. This work is important for advancing the various technological applications of $Na_2Ta_4O_{11}$, and it offers strategies to synthesize other non-layer metal oxide materials.

Acknowledgements

The work gratefully acknowledged financial support from the National Natural Science Foundation of China (Nos. 21975067, 21705036), Natural Science Foundation of Hunan Province, China (No. 2018JJ3035).

References

[1] Machida M, Yabunaka J I, Kijima T. Efficient photocatalytic decom-

position of water with the novel layered tantalate $RbNdTa_2O_7$. Chem Commun, 1999, 30(15), 1939

[2] Tanaka T, Nojima H, Yamamoto T, et al. Structure of surface tantalate species and photo-oxidation of carbon monoxide over silica-supported tantalum oxide. Phys Chem Chem Phys, 1999, 1(22), 5235

[3] Suzuki S, Saito H, Yubuta K, et al. Growth of millimeter-sized platy single crystals of $NaTaO_3$ from Na_2MoO_4 flux. Cryst Growth Des, 2019, 19(7), 3607

[4] Ivanova I, Kandiel T A, Cho Y J, et al. Mechanisms of photocatalytic molecular hydrogen and molecular oxygen evolution over La-doped $NaTaO_3$ particles: effect of different cocatalysts and their specific activity. ACS Catal, 2018, 8(3), 2313

[5] Sudrajat H, Zhou Y, Sasaki T, et al. The atomic-scale structure of $LaCrO_3$–$NaTaO_3$ solid solution photocatalysts with enhanced electron population. Phys Chem Chem Phys, 2019, 21, 5148

[6] Kishimoto K, Yoshio M, Mukai T, et al. Nanostructured anisotropic ion-conductive films. J Am Chem Soc, 2003, 125(11), 3196

[7] Su Y G, Yang X, Wang T T, et al. Sol-gel synthesis of $Na_2Ta_4O_{11}$ nanocrystals showing high efficient photocatalytic performance. Adv Mater Res, 2014, 1058, 35

[8] Mattes R, Schaper J. Crystal structure of $Na_2Ta_4O_{11}$. Revue de Chimie Minerale, 1985, 22(6), 817

[9] Ratnamala, A, Suresh, G, Kumari, V, et al. Template synthesized nano-crystalline natrotantite: preparation and photocatalytic activity for water decomposition. Mater Chem Physs, 2008, 110, 176

[10] McLamb N, Sahoo P P, Fuoco L, et al. Flux growth of single-crystal $Na_2Ta_4O_{11}$ particles and their photocatalytic hydrogen production. Cryst Growth Des, 2013, 13(6), 2322

[11] Teshima K, Tomomatsu D, Suzuki T, et al. Growth of $Na_2Ta_4O_{11}$ crystals from a $Na_2Mo_2O_7$ flux. Cryst Growth Des, 2006, 6(1), 18

[12] Kim Y, Kim S, Lee W H, et al. Direct transfer of CVD-grown graphene onto eco-friendly cellulose film for highly sensitive gas sensor. Cellulose, 2020, 27(3), 1685

[13] Kumar D, Ghadai R K, Das S, et al. Effect of nitrogen flow rate on the mechanical properties of CVD-deposited SiCN thin films. Bull Mater Sci, 2019, 42(5), 251

[14] Jin Y, Zeng Z, Xu Z, et al. Synthesis and transport properties of degenerate p-type Nb-doped WS_2 monolayers. Chem Mater, 2019, 31(9), 3534

[15] Kwon K C, Kim C, Le Q V, et al. Synthesis of atomically thin transition metal disulfides for charge transport layers in optoelectronic devices. ACS Nano, 2015, 9(4), 4146

[16] Ko K Y, Lee S, Park K, et al. High-performance gas sensor using a large-area $WS_{2x}Se_{2-2x}$ alloy for low-power operation wearable applications. ACS Appl Mater Interfaces, 2018, 10(40), 34163

[17] Wang S, Rong Y, Fan Y, et al. Shape evolution of monolayer MoS_2 crystals grown by chemical vapor deposition. Chem Mater, 2014, 26(22), 6371

[18] Harb M, Masih D, Ould-Chikh S, et al. Determination of the electronic structure and UV–Vis absorption properties of $(Na_{2-x}Cu_x)Ta_4O_{11}$ from first-principle calculations. J Phys Chem C, 2013, 117(34), 17477

[19] Palasyuk O, Palasyuk A, Maggard P A. Site-differentiated solid solution in $(Na_{1-x}Cu_x)_2Ta_4O_{11}$ and its electronic structure and optical properties. Inorg Chem, 2010, 49(22), 10571

[20] Mobin M, Malik A. Studies on the interactions of transition metal oxides and sodium sulfate in the temperature range 900–1200 K in oxygen. J Alloy Compd, 1996, 235, 97

[21] Muñoz-Márquez M A, Zarrabeitia M, Castillo-Martínez E, et al. Composition and evolution of the solid-electrolyte interphase in $Na_2Ti_3O_7$ electrodes for Na-ion batteries: XPS and auger parameter analysis. ACS Appl Mater Interfaces, 2015, 7(14), 7801

[22] Kotsis K, Staemmler V. Ab initio calculations of the O1s XPS spectra of ZnO and Zn oxo compounds. Phys Chem Chem Phys, 2006, 8(13), 1490

[23] Grilli R, Simpson R, Mallinson C, et al. Comparison of Ar^+ monoatomic and cluster ion sputtering of Ta_2O_5 at different ion energies, by XPS: Part 2-cluster ions. Surf Sci Spectra, 2014, 21, 68

[24] Van Ngoc H, Qian Y, Han S K, et al. PMMA-etching-free transfer of wafer-scale chemical vapor deposition two-dimensional atomic crystal by a water soluble polyvinyl alcohol polymer method. Sci Rep, 2016, 6(1), 33096

[25] Ithurria S, Talapin D V. Colloidal atomic layer deposition (c-ALD) using self-limiting reactions at nanocrystal surface coupled to phase transfer between polar and nonpolar media. J Am Chem Soc, 2012, 134(45), 18585